Hindawi
Journal of Nanotechnology
Volume 2023, Article ID 8884113, 16 pages
https://doi.org/10.1155/2023/8884113

Research Article

Separation of Spherical Nanosilica from Agricultural Wastes in Vietnam via Ultrasonic-Assisted Precipitation and Application for Effective Removal of Methylene Blue from Aqueous Solution

Nguyen Duc Vu Quyen,[1] Tran Ngoc Tuyen,[1] Dinh Quang Khieu,[1] Ho Van Minh Hai,[1] Dang Xuan Tin,[1] Bui Thi Hoang Diem,[1] Le Van Thanh Son,[2] Nguyen Thi Kieu Diem,[3] Le Thi Nguyet,[4] Bui Thi Thuy,[5] and Ho Thi Thuy Dung[6]

[1]*Department of Chemistry, University of Sciences, Hue University, 77 Nguyen Hue Str., Hue City, Vietnam*
[2]*University of Education and Science, University of Da Nang, 459 Ton Duc Thang Str., Da Nang City, Vietnam*
[3]*Chu Van An High School, Tu Nghia District, Quang Ngai, Vietnam*
[4]*Pleiku High School, Pleiku City, Gia Lai Province, Vietnam*
[5]*Nguyen Du High School, Pleiku City, Gia Lai Province, Vietnam*
[6]*Hue Medical College, 01 Nguyen Truong to Str., Hue City, Vietnam*

Correspondence should be addressed to Nguyen Duc Vu Quyen; ndvquyen@hueuni.edu.vn

Received 5 July 2023; Revised 26 August 2023; Accepted 2 September 2023; Published 26 September 2023

Academic Editor: Marco Rossi

Agricultural wastes including bagasse and rice husk ashes are employed for synthesizing spherical nanosilica materials via the ultrasonic-assisted precipitation process in the present study. The comparison between them and nanosilica prepared from pure sodium silicate is also carried out. The role of the NH_4OH : ethanol volume ratio is demonstrated. The obtained nanosilica is characterized by modern methods including X-ray diffraction (XRD), energy-dispersive X-ray spectroscopy (EDS), infrared spectroscopy (IR), scanning electron microscopy (SEM), and nitrogen adsorption/desorption isotherms (BET). The nanosilica material is employed as an effective adsorbent for the removal of methylene blue (MB) from an aqueous solution. The suitable pH and adsorbent dosage are determined at 8 and 0.375 $g{\cdot}L^{-1}$. The adsorption isotherm study is surveyed based on Langmuir and Freundlich isotherm models. Pseudo-second-order kinetic model and Weber–Morris intraparticle diffusion model well describe the chemical nature of the adsorption. The thermodynamic parameters of the reaction are determined based on the Van't Hoff equation.

1. Introduction

Water pollution is one of the serious and urgent problems not only in Vietnam but also globally, which is increasingly threatening human life and health because most rivers, ponds, and lakes in large urban areas are heavily polluted. One of the notable problems is the existence of toxic and nonbiodegradable organic pigments used in the dyeing industry that is able to accumulate in the organism and cause acute and chronic toxicity for human [1, 2]. Therefore, the treatment of these pollutants in wastewater is a hot issue in recent decades, and scientists have been studying to establish treatment technology for polluted water such as adsorption [3–5], biology combined oxidation-adsorption, or biology [6–11]. Among them, adsorption is proven to be a method with many advantages such as low cost, simplicity, and high efficiency [6–8, 12–14]. The adsorbents used are nontoxic and environmentally friendly.

Nanosilica has a large adsorption capacity for many adsorbents due to its high porosity and surface area and small density which is controlled easily by the synthesis process. Besides, nanosilica is insoluble in all solvents, nontoxic, and odorless. Therefore, nanosilica has been widely known for many practical applications such as catalyst and catalyst

carrier, biomedical application [15–17], adsorbent for wastewater treatment [18–21], petroleum extraction/adsorption or oil spill recovery [22–27], light construction materials [28–30], and bactericide in agriculture [31, 32]. Especially, the use of nanosilica materials for pollutants adsorption from aqueous solution is one of the current interesting methods of environmental pollution treatment [18–21].

The sources used for the synthesis of nanosilica can be natural such as rice husk, bagasse, coir, and mud [15, 16, 33] or pure chemicals such as sodium silicate salt and tetraethyl orthosilicate (TEOS) [34]. Nanosilica synthesized from pure chemicals usually exhibits uniform particle size and high purity resulting in particles that do not agglomerate into larger particles [34]. This is one of the important properties of nanomaterials. Besides, its large surface area leads to high adsorption capacity. However, the obtained nanosilica will be a high-cost product. From this limitation, many researches on the synthesis of nanosilica from cheap raw materials are performed [35].

In Vietnam and many agricultural countries, rice husk and bagasse are cheap and quality sources for nanosilica extraction [36, 37]. These redundant agricultural wastes are discharged in all provinces and villages where they are mainly used as domestic raw fuel. The secondary waste of rice husk ash (RHA) and bagasse ash (BA) is responsible for domestic water pollution [38]. Therefore, studies on the formation of useful nanosilica from RHA (RHA-SiO_2) and BA (BA-SiO_2) are necessary.

Among the silica synthesis methods, precipitation is proven to be easy and effective. In comparison with other methods, it offers the high purity of silica, the simplicity at low temperatures in cheap equipment, the time saving, and the low cost of the product [35, 39, 40]. However, the morphology and particle size could not be controlled with the only common precipitation agent of acid.

In previous studies, the comparison of the structure and adsorption capacity of pollutants from aqueous solution between spherical RHA-SiO_2 and BA-SiO_2 has not been made fully [15, 16, 36, 39, 41]. In this study, nanosilica is separated from rice husk and bagasse collected from Phu Vang district, Thua Thien Hue province, Vietnam, by ultrasonic-assisted precipitation process with the appearance of mixture of NH_4OH : ethanol. The nature of the methylene blue adsorption process onto the obtained material is clarified. Besides, the comparison of the characteristics of two obtained nanosilica materials with this material prepared from pure sodium silicate and their methylene blue (MB) adsorption capacity is carried out.

2. Experimental Setup

2.1. Materials. Rice husk and bagasse were collected in Phu Vang district, Thua Thien Hue province, Vietnam. After being washed with water, the rice husk and bagasse were dried and calcined at 500°C for 3 hours to obtain RHA and BA.

Liquid glass solution was synthesized from ash by soaking the ash in NaOH (Sigma-Aldrich) solution with the molar ratio of $NaOH/SiO_2$ of 1.2 (for BA) and 1.5 (for RHA) and NaOH concentration of 2.2 M. Nanosilica particles were prepared from liquid glass solution by precipitation method as shown in Schema 1. Under strong stirring, a mixture of NH_4OH : ethanol with a defined volume ratio was slowly added to the liquid glass solution. Then, a 1 : 1 HCl solution (by volume) was slowly added to it until the precipitate was completely formed. The mixture was further sonicated for 1 hour using a 400 W ultrasonic bath with a frequency of 37 kHz at 40°C. The fine precipitate was filtered and washed using distilled water to a pH of 7. Nanosilica particles were obtained after drying the precipitate at 80°C for 24 hours.

2.2. Methods

2.2.1. Characterization of Material. X-ray diffraction (XRD) was employed to express the crystal phase of the obtained nanosilica using RINT2000/PC device (Rigaku, Japan) with the tube anode made by Cu with $K_\alpha = 1.54$ Å, and the pattern was obtained at 40 kV of tube voltage and 40 mA of tube current in step scan mode (step size of 0.0297°). The existence of elements in nanosilica was checked from the energy-dispersive X-ray spectrum (EDS) using a Hitachi S4800 device (Japan). The material's morphology was observed through scanning electron microscopy (SEM) (Hitachi S4800, Japan). The porosity of the material was confirmed by the N_2 adsorption and desorption method using a Tristar-3030 system (Micromeritics, USA). A Fourier transform infrared (FT-IR) spectrometer (model IRPrestige-21; Shimadzu, Kyoto, Japan) was used to detect the functional groups on the surface of nanosilica.

2.2.2. Determination of Methylene Blue. Methylene blue (MB) concentration was determined by UV-Vis molecular absorption spectrometry at the wavelength of 660 nm using a Cary 60 UV-Vis (Agilent). The standard curve equation expresses a good linear correlation between absorbance (Abs) and investigates methylene blue concentration (C_{MB}) ($Abs = 0.1384.C_{MB} - 0.0121$) with a very high determination coefficient (0.994).

2.2.3. Determination of Zero Charge Point. The zero charge point (PZC) is a value indicating the pH at which the charge on the surface of the material is zero. This value is determined by using the pH drift method [42]. Nine beakers containing 20 mL of 0.1 M NaCl solutions were prepared with the initial pH value (pH_i) from 2 to 10 which is adjusted by 0.1 M NaOH or 0.1 M HCl solutions. Distilled water was added into the flask until the total volume of the solution was 25 mL. After that, 0.1 g of nanosilica was added to each flask. The mixtures were continuously stirred (200 rpm) for 48 hours. The final pH (pH_f) of the solutions was measured to obtain the value of ΔpH ($\Delta pH = pH_i - pH_f$). The plot between ΔpH and pH_i was obtained. The intersection point of the curve with the horizontal axis is the value of PZC.

2.2.4. Determination of Ultrasonic Time. The ultrasonic time is investigated from 30 to 180 minutes. All the nanosilica materials synthesized with different ultrasonic times are

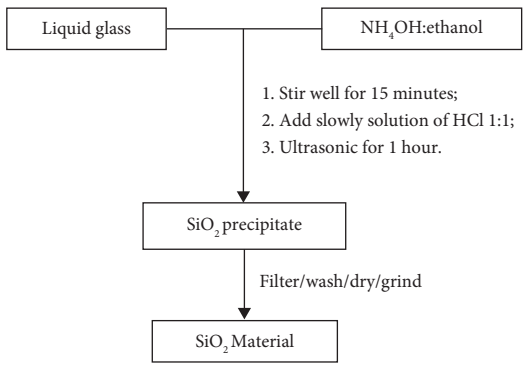

Schema 1: The synthesis process of nanosilica from liquid glass prepared from RHA and BA.

used to remove MB from an aqueous solution with an MB initial concentration of 10 mg·L^{-1} at a pH of 6 for 120 mins, and the suitable time is chosen based on their adsorption efficiency of MB.

2.2.5. Adsorption Studies. The pH of the solution, adsorbent dosage, initial MB concentrations, solution temperature, and contact time were surveyed in batch experiments. The mixtures consisting of 20 mL of MB solution and nanosilica with the adsorbent dosage of 0.5 g·L^{-1} were prepared in ten flasks, and the pH of the solution was adjusted from 2 to 11 by HNO_3 (0.1 mol·L^{-1}) and NaOH (0.1 mol·L^{-1}), sequentially. All the samples were performed under stirring (300 rpm) at 30°C for 120 mins with the aim of reaching the adsorption equilibrium. The remaining MB concentration of each sample was determined for calculating adsorption efficiency. The experiment was taken place again with the stable pH chosen from the above investigation, and the adsorbent dosage was varied from 0.25 to 0.75 g·L^{-1}.

For the adsorption isotherm study, the adsorption capacity was calculated at different initial MB contents from 10 to 50 mg·L^{-1}, and Langmuir and Freundlich isotherm models were employed for describing the experimental data. MB monolayer adsorption capacity was inferred from the Langmuir model.

The adsorption kinetic study was carried out in 250 mL of MB solution with a defined dosage of adsorbent. Every 10 minutes, 10 mL of the mixture including both MB solution and adsorbent was sucked out for determining the remaining MB content. The experimental data were analyzed using the first-order and second-order kinetic models, and Weber–Morris intraparticle diffusion model.

Thermodynamic parameters were determined from the effect of temperature (from 283 to 333K) on MB adsorption capacity using the Van't Hoff plot.

3. Results and Discussion

3.1. Preparation of RHA and BA. With the aim of eliminating the influence of metal impurities, the ashes were treated with 1M HCl solution for 24 hours. The EDS spectra of RHA and BA as shown in Figures 1 and 2 express that most of the main metals are removed from two kinds of ashes.

The EDS analyses were performed on three different samples of each kind of ash ($n = 3$). The weight percentages of the elements between the three samples of each kind of ash are not much different, as shown in the small values of relative standard deviation. The SiO_2 content of RHA and BA determined is 49.54% and 79.80%, respectively.

3.2. Effect of Volume Ratio of NH_4OH : Ethanol on the Morphology of Nanosilica. One of the disadvantages of the precipitation method is the formation of polystructural silica clusters with undefined particle shapes and large particle sizes. The morphology and particle size of nanosilica strongly depend on the conditions of the synthesis process and can be controlled by the existence of solvent. The effect of NH_4OH : ethanol volume ratio on the material morphology was investigated in the present study. For comparison and choice of suitable NH_4OH : ethanol volume ratio, RHA-SiO_2, BA-SiO_2 nanoparticles, and nanosilica synthesized from pure Na_2SiO_3 (pure-SiO_2) were obtained with different ratios as shown in Figures 3–5. Ultrasonic time is fixed at 60 minutes.

SEM images in Figures 3 and 4 show that NH_4OH : ethanol volume ratio expresses a great influence on the formation of spherical particle structure of RHA-SiO_2 and BA-SiO_2 nanomaterials. During the synthesis without the mixture of NH_4OH and ethanol at the early stage, spherical nanosilica was unformed, and the amorphous structure was obtained instead. Meanwhile, the nanometer-sized spherical particle structure of pure-SiO_2 nanomaterial (Figure 5) was formed at all volume ratios of NH_4OH : ethanol. However, the absence of the mixture of NH_4OH and ethanol (Figure 5(o)) resulted in the incomplete formation of spherical nanoparticles, ununiform particle size, and the agglomeration of many particles into large clumps. The more volume of NH_4OH in the mixture was, the more complete and round silica nanoparticles were. It is predicted that the bad influence of impurities in the liquid glass solution separated from rice husk ash and bagasse ash is excluded because of the existence of NH_4OH and ethanol mixture at a suitable volume ratio. The suitable volume ratio of NH_4OH : ethanol of 12 : 3 gave well-shaped particles with clear grain boundaries, smooth surface, and uniform diameter from 100 to 150 nm (Figure 5(t)).

For both natural sources (Figures 3 and 4), in the sample synthesized with ethanol but without NH_4OH, the spherical particles did not appear that confirms the important role of NH_4OH. When increasing the amount of NH_4OH corresponding to NH_4OH : ethanol volume ratio from 3 : 12 to 15 : 0, the spherical particles in samples gradually achieved and increased in number. Nanosilica particles are partly formed with clear grain boundaries, smooth surface at the ratio of 6 : 9, and wholly at the ratio of 13 : 2. Both materials obtained at NH_4OH : ethanol volume ratio of 13 : 2 exhibit uniform particle size in the range of 150–200 nm. Nevertheless, when ethanol was absent in the mixture (Figures 3(g) and 4(n)), some particles were agglomerated into clusters which reduced surface area. This demonstrates the important role of ethanol in preventing nanosilica particles from agglomerating.

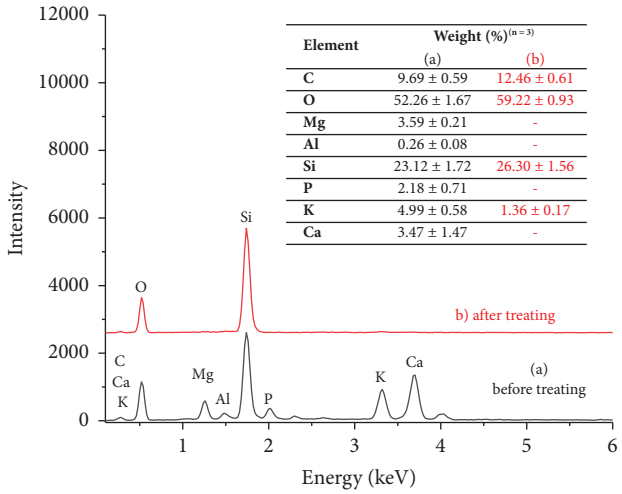

Element	Weight (%)$^{(n=3)}$ (a)	(b)
C	9.69 ± 0.59	12.46 ± 0.61
O	52.26 ± 1.67	59.22 ± 0.93
Mg	3.59 ± 0.21	-
Al	0.26 ± 0.08	-
Si	23.12 ± 1.72	26.30 ± 1.56
P	2.18 ± 0.71	-
K	4.99 ± 0.58	1.36 ± 0.17
Ca	3.47 ± 1.47	-

Figure 1: EDS analyses of bagasse ash before (a) and after (b) treated by HCl 1M.

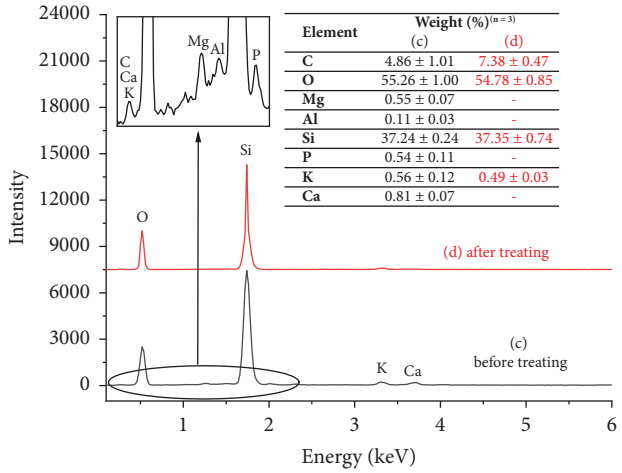

Element	Weight (%)$^{(n=3)}$ (c)	(d)
C	4.86 ± 1.01	7.38 ± 0.47
O	55.26 ± 1.00	54.78 ± 0.85
Mg	0.55 ± 0.07	-
Al	0.11 ± 0.03	-
Si	37.24 ± 0.24	37.35 ± 0.74
P	0.54 ± 0.11	-
K	0.56 ± 0.12	0.49 ± 0.03
Ca	0.81 ± 0.07	-

Figure 2: EDS analyses of rice husk ash before (c) and after (d) treated by HCl 1M.

Setyawan et al. [41] also extracted silica from RHA by sol-gel method with the same precipitating agent of HCl solution. However, the lack of NH_4OH : ethanol mixture seems to be the reason causing the fact that silica appeared agglomerate and was not a single particle. Noushad et al. [39] employed ethanol as a nonpolar solvent and orthophosphoric acid as a precipitating agent to obtain silica from RHA with ununiform spherical particle diameters from 80 to 360 nm. Besides, almost of particles are observed in cluster. From sugarcane bagasse, Athinarayanan et al. [16] synthesized biogenic silica nanoparticles using HCl pretreatment and calcination at 750°C. The unemployment of NH_4OH : ethanol solvent results in large clusters in undefined shapes with an average size of 191 nm. In another study, amorphous silica was separated from BA and RHA using H_2SO_4 as a precipitating agent and without NH_4OH : ethanol solvent [43]. The result showed that silica particles exhibited undefined shapes with various sizes and agglomerated. In conclusion, there are few differences between nanosilica separated from two kinds of the above natural source. The results conclude that the suitable NH_4OH : ethanol volume ratio is 12 : 3.

3.3. Effect of Ultrasonic Time on MB Adsorption Efficiency. The ultrasonic technique is an effective way for particle dispersion and deagglomeration of nanomaterials during their synthesis process [44]. The ultrasound energy causes the formation, growth, and collapse of cavitation bubbles in the liquid medium. Under the violent collapse of acoustic cavitation bubbles, hydrogen and hydroxyl radicals are formed, which prevents the agglomeration of nanoparticles [45]. The adsorption efficiency of MB increases significantly from 38.1% without the ultrasonic process to 68.0% with 30 mins of ultrasonic time. Then, the longer the ultrasonic time is, the higher the adsorption efficiency is. After 60 minutes of ultrasonic time, most of the MB is removed from the aqueous solution (adsorption efficiency of around 97%).

3.4. Characterization of Nanosilica. The XRD patterns expressed in Figure 6 expose the crystalline nature of the obtained nanosilica in the range of 2θ from 10° to 70°. The only broad peak at 2θ of 22° appearing in three XRD spectra of RHA-SiO_2, BA-SiO_2, and pure-SiO_2 nanomaterials corresponds to amorphous phase SiO_2 [16, 42, 43, 46].

The morphology of the best nanosilica samples was observed on SEM images as shown in Figures 3(f), 4(m), and 5(t). The spherical particles with clear grain boundaries, smooth surface, no agglomeration, and uniform diameter of about 100–150 nm appeared in sample separated from pure chemical, and 150–200 nm was obtained in two samples made from natural sources.

The porosity of SiO_2 materials was evaluated by the N_2 adsorption and desorption method. According to the IUPAC classification, the adsorption and desorption curves of the materials as shown in Figure 7 are confirmed in IV type corresponding to the adsorption of micromesoporous material. The form of hysteresis curves means the mesopores created among SiO_2 nanoparticles are disordered. It is predicted that the pore cavity distribution is wide compared with the neck size distribution [47]. The hysteresis curve of pure-SiO_2 nanomaterial (Figure 7(c)) ($P/P_o \sim 0.6$) appears at the higher pressure in comparison with RHA-SiO_2 nanomaterial (Figure 7(b)) and BA-SiO_2 nanomaterial (Figure 7(a)) ($P/P_o \sim 0.4$). This confirms that the pore neck size of pure-SiO_2 nanomaterial is smaller than that of RHA-SiO_2 and BA-SiO_2 nanomaterials. The smaller the particle size is, the narrower the pore neck size is.

The pore volume distribution of the materials expressed according to the Barrett–Joyner–Halenda (BJH) model is shown in Figure 8. As can be seen, the pore size of the material concentrates in the range from 2 to 10 nm for all 3 samples. The BET surface area of pure-SiO_2, RHA-SiO_2, and BA-SiO_2 nanomaterials is 214.0, 180.6, and 187.5 $m^2 \cdot g^{-1}$, respectively. It is found that the BET surface areas of SiO_2 nanomaterials synthesized from natural sources are similar together and significantly lower than those of SiO_2 nanomaterials made from pure Na_2SiO_3. This could be due to the impurities of RHA and BA.

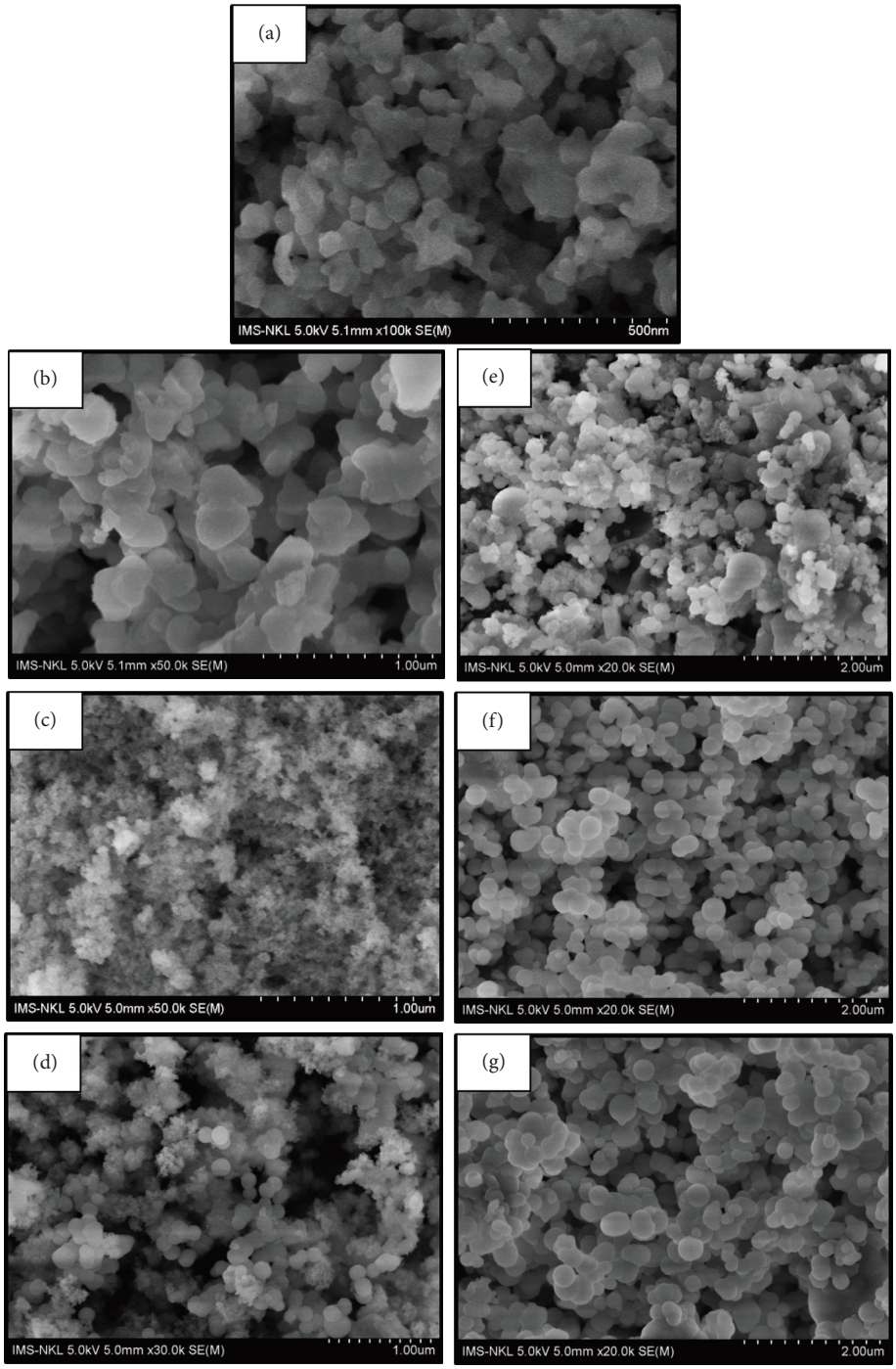

FIGURE 3: The morphology of BA-SiO_2 nanomaterial with different volume ratios of NH_4OH : ethanol: (a) 0 : 0; (b) 0 : 15; (c) 3 : 12; (d) 6 : 9; (e) 9 : 6; (f) 12 : 3; (g) 15 : 0.

The elemental composition of RHA-SiO_2 and BA-SiO_2 nanomaterials inferred from their EDS spectra as shown in Figure 9 confirms the main elements of Si and O corresponding to the main chemical composition of SiO_2.

The functional groups on the surface of nanosilica were confirmed on FT-IR spectra as shown in Figure 10. The O-H groups are detected based on stretching vibration noticed at the broadband from 3000 to 3700 cm^{-1} and the peak of

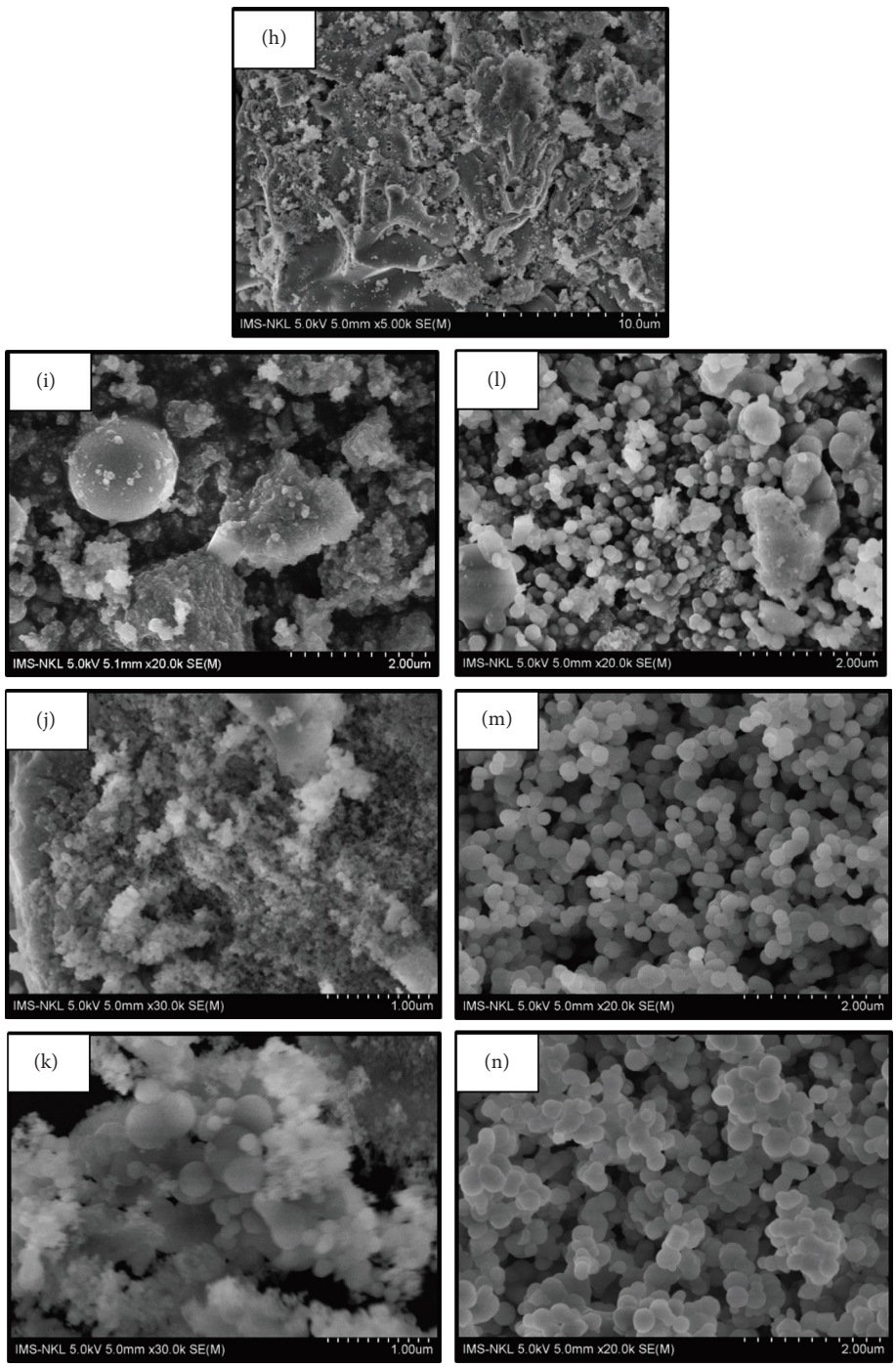

Figure 4: The morphology of RHA-SiO_2 nanomaterial with different volume ratios of NH_4OH : ethanol: (h) 0 : 0; (i) 0 : 15; (j) 3 : 12; (k) 6 : 9; (l) 9 : 6; (m) 12 : 3; (n) 15 : 0.

1631 cm^{-1}. The presence of the peak at 1099 and 464 cm^{-1} relating to the bending variations of Si-O-Si and 952 cm^{-1} assigned to stretching vibrations of Si-OH demonstrates the existence of Si element in the material [48, 49].

One of the important characteristics of the adsorbent is its zero charge point. Figure 11 shows the data for the determination of the zero charge point of BA-SiO_2 (a), RHA-SiO_2 (b), and pure-SiO_2 (c) nanomaterials following the

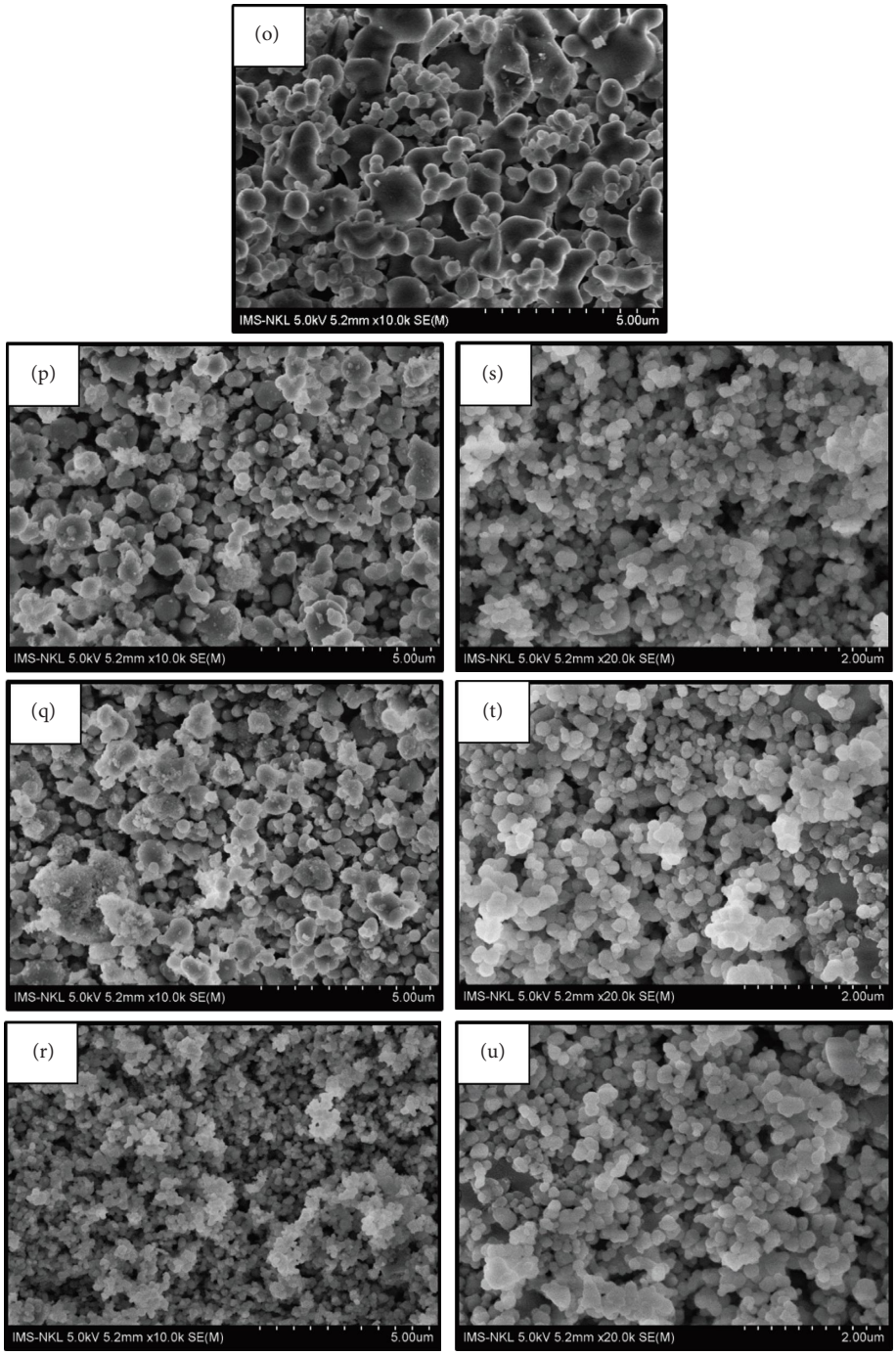

FIGURE 5: The morphology of pure-SiO_2 nanomaterial with different volume ratios of NH_4OH : ethanol: (o) 0 : 0; (p) 0 : 15; (q) 3 : 12; (r) 6 : 9; (s) 9 : 6; (t) 12 : 3; (u) 15 : 0.

description in item 2.2.3. The zero charge points of all materials are in the range of 3 to 3.3.

3.5. Adsorption Study of Methylene Blue onto BA-SiO_2, RHA-SiO_2, and Pure-SiO_2 Nanomaterials

3.5.1. Effect of pH. The results expressed that MB adsorption efficiency is strongly dependent on pH. When the pH of the solution increases from 2 to 8, the MB adsorption efficiency rapidly enhances and then slightly rises for BA-SiO_2 sample, or insignificantly changes for RHA-SiO_2 and pure-SiO_2 samples. This indicates a pH of 8 or higher which is favorable for MB adsorption. With the initial MB concentration of 20 $mg \cdot L^{-1}$ and adsorbent dosage of 0.25 $g \cdot L^{-1}$, the MB adsorption efficiency at pH of 8 was 88.9%, 83.4%, and 93.5% for BA-SiO_2, RHA-SiO_2, and pure-SiO_2 samples, respectively. It is assumed that the purity of SiO_2 seems to be one of the factors causing the lightly higher adsorption efficiency of

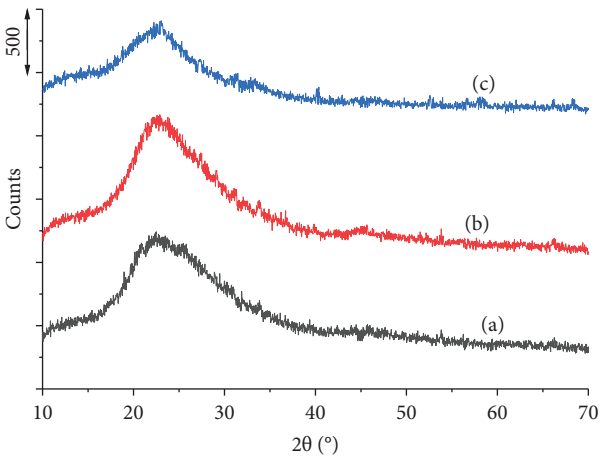

Figure 6: XRD spectra of BA-SiO_2 (a), RHA-SiO_2 (b), and pure-SiO_2 (c) nanomaterials.

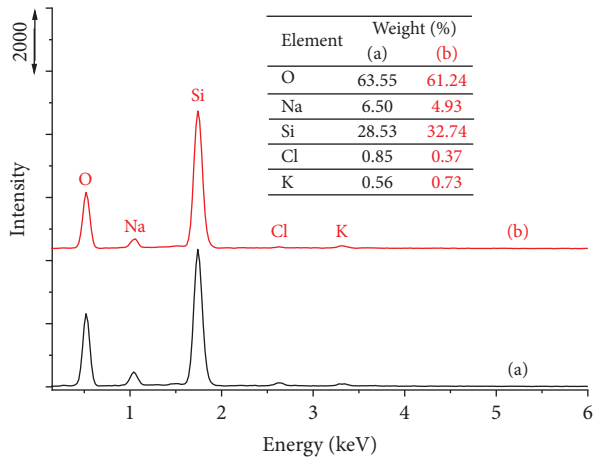

Element	Weight (%) (a)	(b)
O	63.55	61.24
Na	6.50	4.93
Si	28.53	32.74
Cl	0.85	0.37
K	0.56	0.73

Figure 9: EDX spectra of BA-SiO_2 (a) and RHA-SiO_2 (b) nanomaterials.

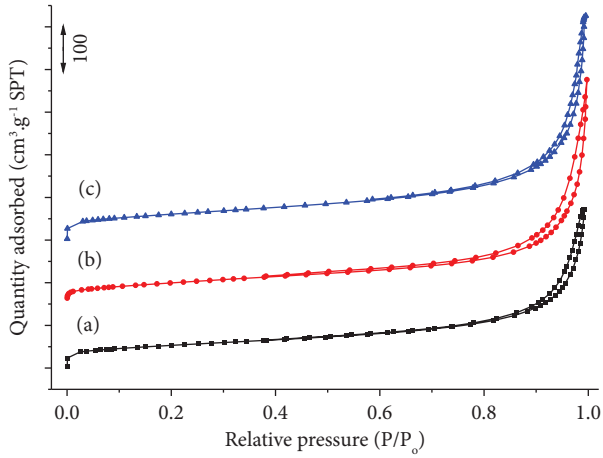

Figure 7: N_2 adsorption and desorption linear plots of BA-SiO_2 (a), RHA-SiO_2 (b), and pure-SiO_2 (c) nanomaterials.

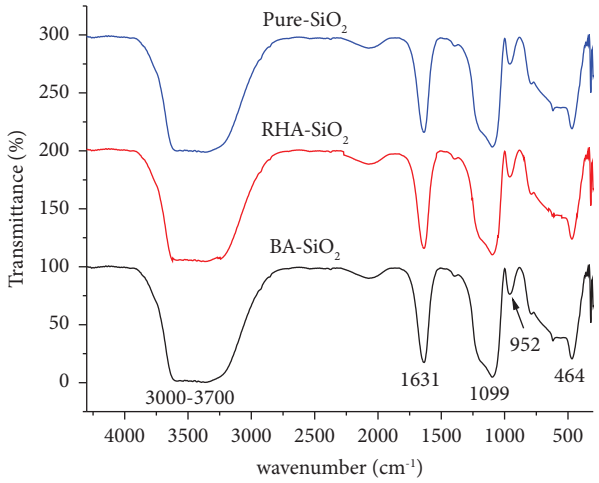

Figure 10: FT-IR study on BA-SiO_2, RHA-SiO_2, and pure-SiO_2 nanomaterials.

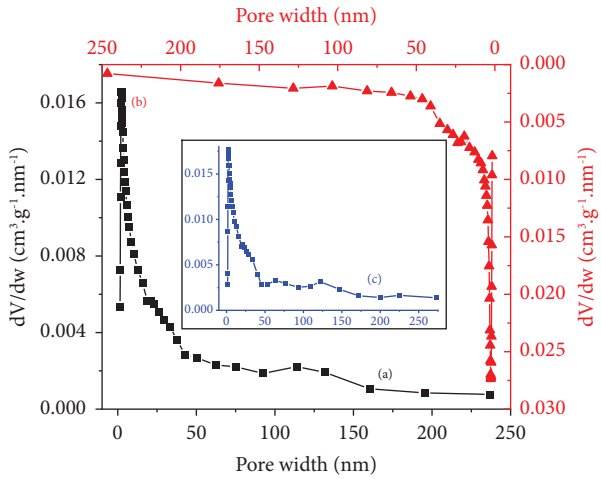

Figure 8: Pore volume distribution of BA-SiO_2 (a), RHA-SiO_2 (b), and pure-SiO_2 (c) nanomaterials.

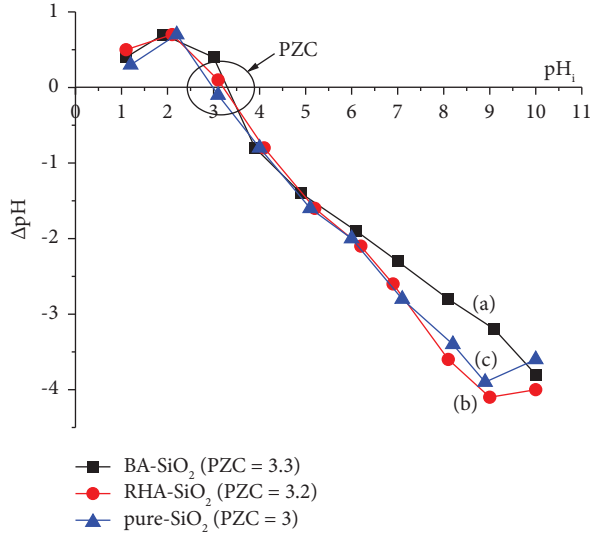

Figure 11: PZC diagram of BA-SiO_2 (a), RHA-SiO_2 (b), and pure-SiO_2 (c) nanomaterials.

pure-SiO_2 sample compared to BA-SiO_2 and RHA-SiO_2 ones. Therefore, it can be seen that the nanosilica made from pure chemicals can be replaced by nanosilica synthesized from natural sources for MB-effective adsorption.

The change in adsorption efficiency with pH could be explained based on the PZC value of the material (PZC ~ 3). At a pH lower than 3, the positive surface of the material prevents MB^+ ions from reaching the material. However, the higher the pH is, the less the positive charge covers the surface. This is explained by the higher adsorption efficiency as the pH of the solution increases from 2 to 3. The surface of the material becomes negative at a pH higher than 3 and gradually rises with pH. Therefore, the adsorption efficiency is rapidly enhanced when increasing pH from 4 to 11 due to the easy attraction of MB^+ ions to the surface of the adsorbent.

3.5.2. Effect of Adsorbent Dosage. With the initial MB concentration of 20 $mg{\cdot}L^{-1}$, at a pH of 8, the dosage of adsorbent was investigated from 0.125 to 0.375 $g{\cdot}L^{-1}$. For all three materials, the adsorption efficiencies achieve more than 80% at the dosage of 0.250 $g{\cdot}L^{-1}$. Then, almost MB is removed from the solution when rising the adsorbent dosage to 0.375 $g{\cdot}L^{-1}$. The adsorption efficiency reaches over 99% for BA-SiO_2 and pure-SiO_2 samples and over 94% for RHA-SiO_2 sample.

3.5.3. Study of Isotherm Adsorption. From the data in Table 1, it can be seen that MB adsorption capacity tends to gradually increase with the rising of initial MB concentration from 10 to 50 $mg{\cdot}L^{-1}$ in the same reaction conditions including the adsorbent dosage of 0.25 g/L for 180 mins at room temperature, at which, the pure-SiO_2 nanoparticles exhibit a rather better adsorption capacity than BA-SiO_2 and RHA-SiO_2 ones.

Langmuir and Freundlich nonlinear isotherm equations have been employed for reviewing the data as shown in (1) and (2) equations which are illustrated in Figure 12 [50]:

$$q_e = \frac{q_m K_L C_e}{1 + K_L C_e}, \tag{1}$$

$$q_e = K_F C_e^{1/n}, \tag{2}$$

where K_L is the Langmuir constant which is related to the strength of adsorption, and K_F and n are the Freundlich constants.

For each material, it is found that the determination coefficient for the Freundlich model is slightly higher than that for the Langmuir model (Table 2). This fact demonstrates that the adsorption is mainly in the multilayer form with a heterogeneous surface. $1/n$ value calculated from the nonlinearized Freundlich equation is between 0 and 0.5, suggesting that the adsorption is favorable [51]. The single-layer adsorption capacity (q_m) inferred from the Langmuir model is all rather higher than some others as shown in Table 3. BA-SiO_2 adsorbent exhibits the highest capacity (214.97 $mg{\cdot}g^{-1}$) in the three obtained materials (169.21 $mg{\cdot}g^{-1}$ for RHA-SiO_2 and 196.78 $mg{\cdot}g^{-1}$ for pure-SiO_2.).

Table 1: Comparison of MB adsorption capacity of BA-SiO_2, RHA-SiO_2, and pure-SiO_2.

Materials		BA-SiO_2	RHA-SiO_2	Pure-SiO_2
C°_{MB} ($mg{\cdot}L^{-1}$)				
	10	41.9	41.2	41.7
	20	73.5	69.9	75.8
q_e ($mg{\cdot}g^{-1}$)	30	99.2	95.0	103.3
	40	137.4	124.1	141.7
	50	154.1	142.5	158.3

3.5.4. Study of Adsorption Kinetics. The insight into the adsorption is provided by the kinetic study including mass transfer, diffusion, and surface adsorption [58]. Accordingly, the adsorption time was investigated until the adsorption reached the equilibrium as shown in Figure 13. As can be seen, for all surveyed adsorbents, the time of adsorption equilibrium is about 45–60 minutes with the initial MB concentration of 10 $mg{\cdot}L^{-1}$.

The increase of initial MB concentration from 20 to 50 $mg{\cdot}L^{-1}$ results in the enhancement of adsorption equilibrium time to about 75–90 minutes. Here, the adsorption equilibrium time of pure-SiO_2 material is shorter (45 minutes for the concentration of 10 and 75 minutes for the remaining concentrations) than that of the other two materials.

For the purpose of clarifying the kinetic nature of MB adsorption onto the synthesized nanosilica materials, Lagergren's first-order (LFO) kinetic model (equation (3)), Ho's second-order (PSO) kinetic model [59] (equation (4)), and Weber–Morris intraparticle diffusion model (IPD) [60] (equation (5)) were applied. These models are given, respectively, as follows:

$$\ln(q_e - q_t) = \ln q_e - k_1 t, \tag{3}$$

$$\frac{t}{q_t} = \frac{1}{k_2 q_e^2} + \frac{t}{q_e}, \tag{4}$$

$$q_t = k_{\text{dif}} t^{1/2} + C, \tag{5}$$

where k_{dif} is the intraparticle diffusion rate constant ($mg{\cdot}g^{-1}{\cdot}min^{-1/2}$), C ($mg{\cdot}mg^{-1}$) is a constant which is related to diffusion resistance and is a characteristic constant for the layer of the solution surrounding the particle, and k_1 and k_2 are Lagergren's first-order and Ho's second-order rate constants, respectively.

The study is carried out at different initial MB contents from 10 to 50 $mg{\cdot}L^{-1}$. As shown in Table 4, when describing the MB adsorption onto three materials, the linear equation of the PSO kinetic model exhibits slightly higher determination coefficients than that of the LFO kinetic model at all initial MB concentrations. Besides, the experimental adsorption capacity value ($q_{e(\text{ex})}$) is quite close to this calculated from the PSO kinetic equation ($q_{e(\text{mo})}$). In other words, the PSO model well depicted the kinetics of MB adsorption onto BA-SiO_2, RHA-SiO_2, and Pure-SiO_2, which confirms the chemisorption process [61]. The adsorption rate depends on both concentrations of adsorbent and adsorbate.

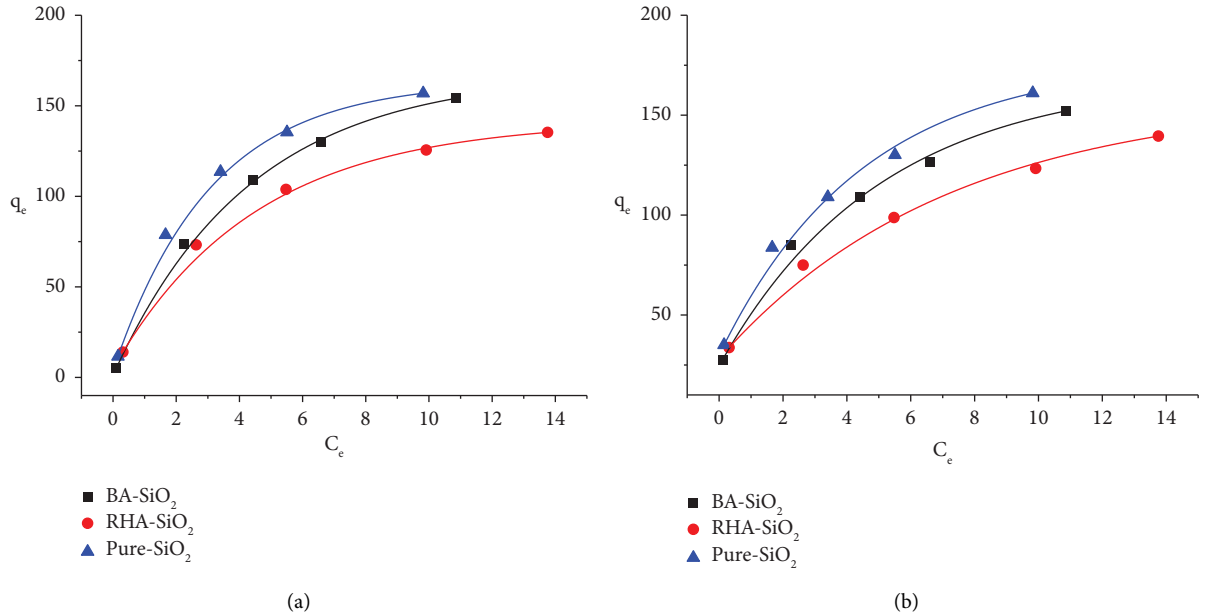

Figure 12: Nonlinearized Langmuir (a) and Freundlich (b) isotherm studies on MB adsorption of BA-SiO_2, RHA-SiO_2, and pure-SiO_2.

Table 2: Isotherm parameters calculated from the Langmuir and Freundlich models of MB adsorption onto BA-SiO_2, RHA-SiO_2, and pure-SiO_2.

Materials		BA-SiO_2	RHA-SiO_2	Pure-SiO_2
Langmuir model	q_m (mg·g^{-1})	214.97	169.21	196.78
	K_L	0.23	0.29	0.40
	R^2	0.821	0.868	0.882
Freundlich model	$1/n$	0.37	0.38	0.37
	K_F	63.09	52.18	69.46
	R^2	0.933	0.984	0.969

Table 3: Comparison of the single-layer adsorption capacity (q_m) of MB on silica adsorbents.

Adsorbent	q_m (mg·g^{-1})	References
BA-SiO_2	214.97	
RHA-SiO_2	169.21	The present work
Pure-SiO_2	196.78	
Rice husk silica	103.11	[52]
Modified nanosilica gel	9.54	[53]
Silica gel derived from Algerian siliceous by-product of kaolin	87.33	[54]
Silica nanospheres synthesized from TEOS	2.89	[55]
Dendritic silica nanoparticles	90.70	[56]
Silica nanoparticles prepared from diatomite	347.20	[57]

The adsorption includes three stages of the diffusion of the adsorbate (i) from the solution to the surface of the adsorbent forming a solution layer surrounding the particle (k_{dif1}) and (ii) from this surface into its intraparticle capillary (k_{dif2}); after that, the final stage is (iii) the adsorption equilibrium. In some cases, such as BA-SiO_2 material or low initial concentration of MB for RHA-SiO_2 and pure-SiO_2 ones, the first and second stages can be taken place simultaneously resulting strong increase in adsorption capacity (Figure 14).

The effect of the solution layer surrounding the particle is evaluated based on the constant C of Weber–Morris intraparticle diffusion as shown in Table 5. The greater this constant is, the thicker this layer is. The thick solution layer will hinder the diffusion of the adsorbate into the intraparticle capillary of the adsorbent.

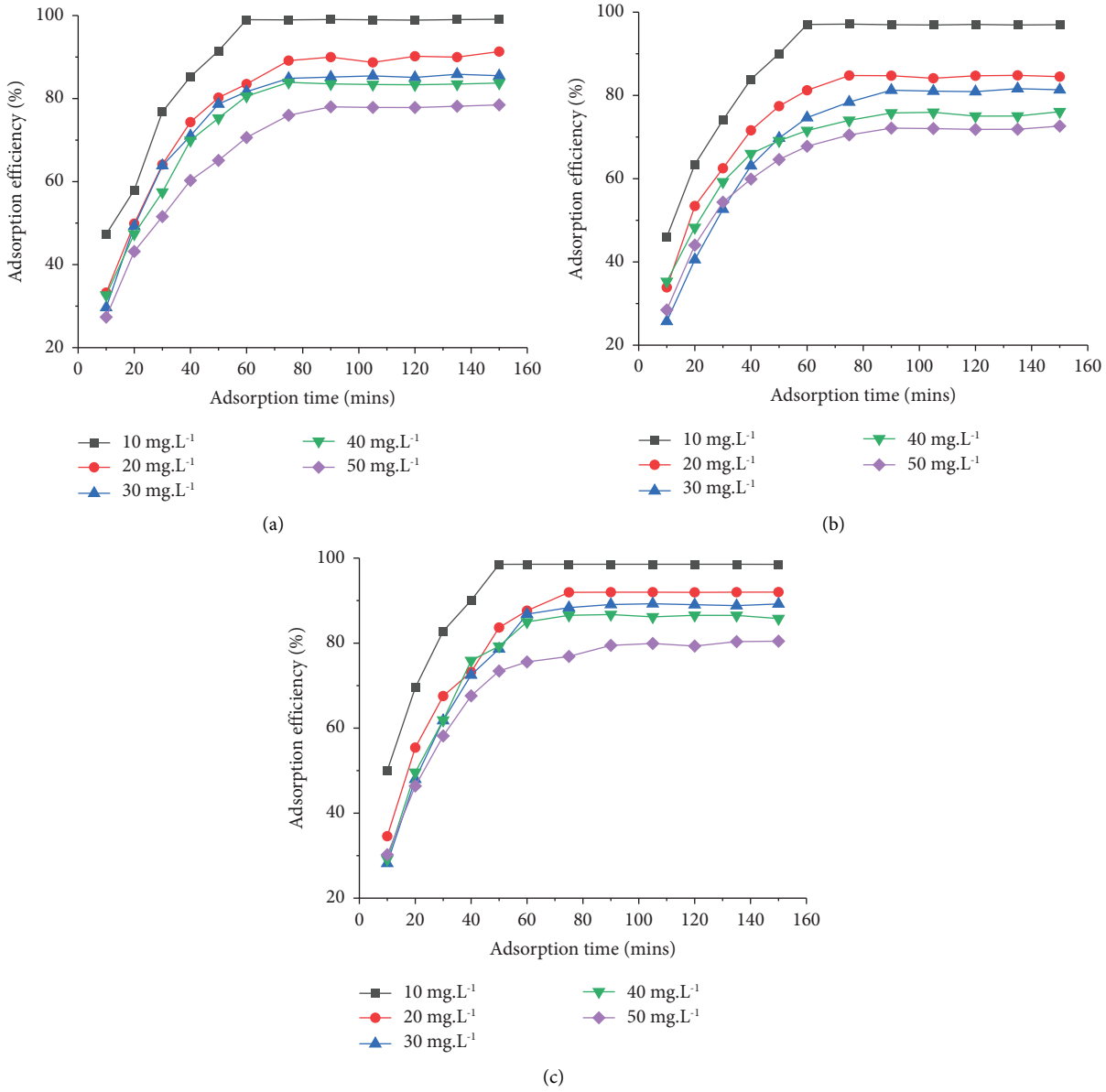

Figure 13: Effect of adsorption time on MB adsorption capacity of BA-SiO_2 (a), RHA-SiO_2 (b), and pure-SiO_2 (c).

For BA-SiO_2 material, at all of the surveyed MB concentrations, in the initial 50–75 minutes, the C value gets closer to zero corresponding to a thin MB solution layer surrounding the material and the fast movement of MB molecules passing through this layer. Therefore, a strong uptrend of MB adsorption capacity is observed as shown in Figure 13(a), and the stage of intraparticle diffusion is predicted as the step determining the rate of MB adsorption. It is found that after 50–75 minutes, the C value is much higher, which means the longer the time is, the thicker the layer is, hindering the diffusion of MB inside the material capillary. As a result, the adsorption capacity value varies unremarkable, and the equilibrium is obtained that seems to indicate that almost of active adsorption sites of material are saturated. Nevertheless, the equilibrium adsorption capacity still augments as a consequence of the rising of MB content from 10 to 50 mg·L^{-1} although the C value gradually increases from 2.62 to 9.40. Besides, it is concluded that the diffusion rate constants of stages (k_{dif}) are seen in a downtrend from k_{dif1} to k_{dif2} from Table 5 because of the simultaneous occurrence of the external and intraparticle diffusions of MB for initial 50–75 minutes (k_{dif1}) and the following equilibrium (k_{dif2}).

Regarding the initial MB concentration from 30 to 50 mg·L^{-1} for RHA-SiO_2 (Figure 13(b)) or from 40 to 50 mg·L^{-1} for pure-SiO_2 (Figure 13(c)), the adsorption process is divided into three stages: the first stage (the initial 30–40 minutes) of the quick adsorption because of a thin boundary layer, which is proved by the C value which is close to zero; the second one (the following 50–75 minutes) corresponding to slower enhance of adsorption capacity caused by the thicker solution layer (higher C value); the

Table 4: Parameters of pseudo-first- and second-order kinetic studies on MB adsorption of BA-SiO_2, RHA-SiO_2, and pure-SiO_2 at different initial MB contents.

MB initial concentrations ($mg{\cdot}L^{-1}$)			10	20	30	40	50
Pseudo-first-order kinetic model	$q_{e(mo)}$ ($mg{\cdot}g^{-1}$)	BA-SiO_2	2.07	4.13	7.01	8.73	10.74
		RHA-SiO_2	3.55	7.92	11.26	10.17	14.47
		Pure-SiO_2	3.56	8.14	17.45	22.37	15.18
	k	BA-SiO_2	0.0448	0.0434	0.0542	0.049	0.0443
		RHA-SiO_2	0.0491	0.0579	0.0459	0.0456	0.0492
		Pure-SiO_2	0.0584	0.0505	0.0661	0.0677	0.0485
	R^2	BA-SiO_2	0.982	0.991	0.981	0.947	0.931
		RHA-SiO_2	0.989	0.974	0.988	0.998	0.991
		Pure-SiO_2	0.998	0.972	0.888	0.940	0.986
Pseudo-second-order kinetic model	$q_{e(mo)}$ ($mg{\cdot}g^{-1}$)	BA-SiO_2	2.84	5.20	6.95	9.44	11.03
		RHA-SiO_2	4.20	7.28	10.63	12.69	14.99
		Pure-SiO_2	4.17	8.04	11.38	15.04	16.78
	k	BA-SiO_2	0.0372	0.0137	0.0108	0.0086	0.0052
		RHA-SiO_2	0.0228	0.0104	0.0041	0.0070	0.0046
		Pure-SiO_2	0.0332	0.0082	0.0046	0.0043	0.0039
	R^2	BA-SiO_2	0.997	0.998	0.996	0.996	0.996
		RHA-SiO_2	0.997	0.996	0.992	0.998	0.997
		Pure-SiO_2	0.997	0.995	0.989	0.989	0.996
$q_{e(ex)}$ ($mg{\cdot}g^{-1}$)		BA-SiO_2	2.62	4.59	6.20	8.59	9.63
		RHA-SiO_2	3.86	6.55	8.90	11.63	13.36
		Pure-SiO_2	3.91	7.10	9.68	13.28	14.72

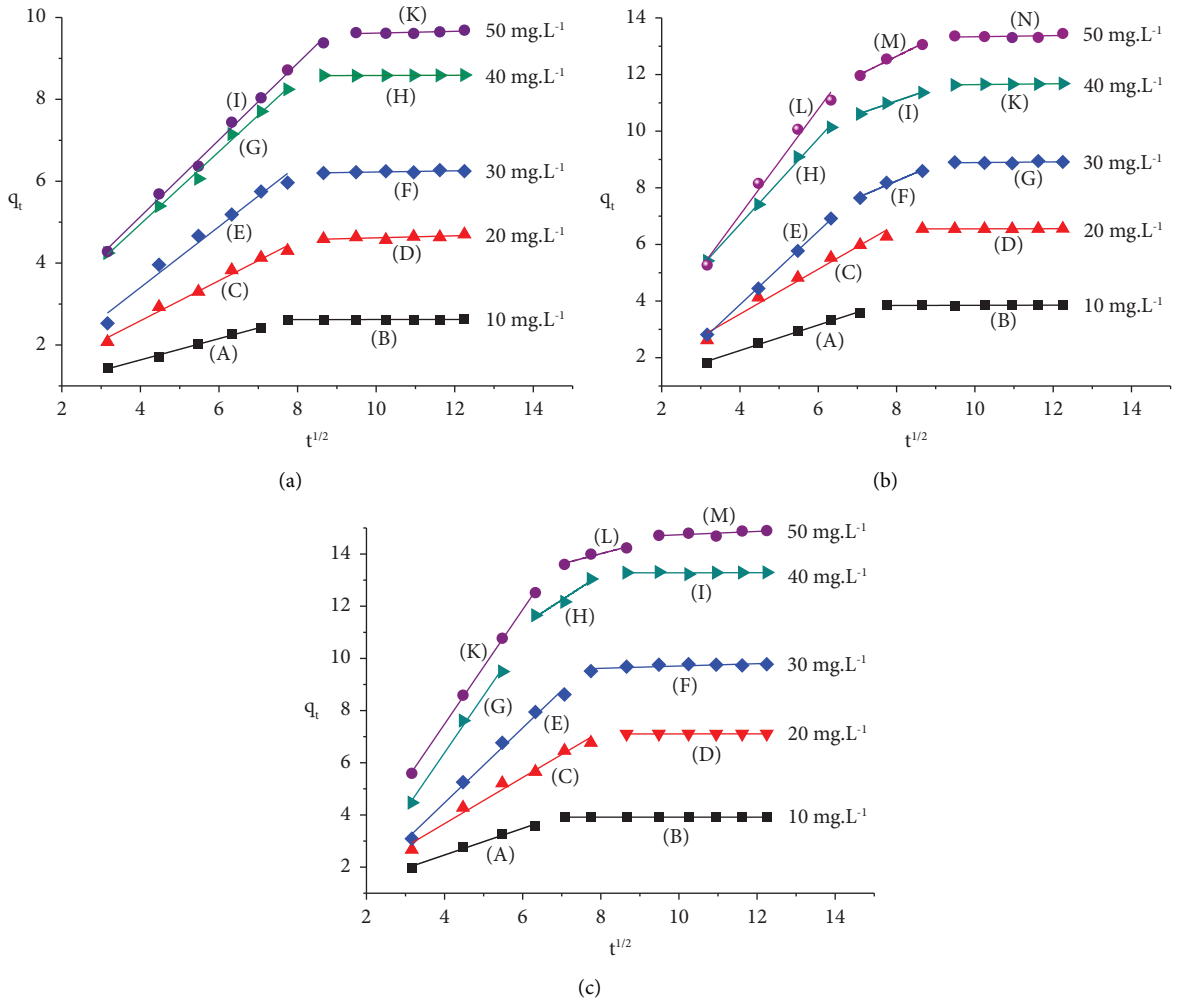

Figure 14: Weber–Morris intraparticle diffusion study on MB adsorption of BA-SiO_2 (a), RHA-SiO_2 (b), and pure-SiO_2 (c).

Table 5: Parameters of Weber–Morris intraparticle diffusion study on MB adsorption of BA-SiO_2, RHA-SiO_2, and pure-SiO_2.

Materials	MB initial concentration ($mg{\cdot}L^{-1}$)	The constant related to diffusion resistance (C)			The intraparticle diffusion rate constant (k_{dif})		
		First stage (C_1)	Second stage (C_2)	Third stage (C_3)	First stage (k_{dif1})	Second stage (k_{dif2})	Third stage (k_{dif3})
BA-SiO_2	10	0.59	2.62		0.260	0.003	
	20	0.63	4.37		0.490	0.025	
	30	0.43	6.08		0.744	0.015	
	40	1.40	8.56		0.886	0.002	
	50	1.39	9.40		0.936	0.022	
RHA-SiO_2	10	0.46	3.82		0.450	0.003	
	20	0.37	6.53		0.793	0.002	
	30	−1.31	3.52	8.77	1.295	0.590	0.012
	40	0.66	7.30	11.50	1.513	0.470	0.015
	50	−0.43	7.19	13.13	1.868	0.681	0.020
Pure-SiO_2	10	0.42	3.91		0.510	10^{-5}	
	20	0.13	7.10		0.884	0.001	
	30	−1.28	9.26		1.435	0.045	
	40	−2.34	5.42	13.27	2.182	0.975	0.001
	50	−1.28	10.88	14.09	2.192	0.391	0.064

Table 6: Thermodynamic parameters of MB adsorption onto BA-SiO_2, RHA-SiO_2, and pure-SiO_2.

Parameters	Materials	Temperature (K) 283	293	303	313	323	333
ΔH° ($kJ{\cdot}mol^{-1}$)	BA-SiO_2			−58.98			
	RHA-SiO_2			−51.95			
	Pure-SiO_2			−59.41			
ΔS° ($J{\cdot}mol^{-1}$)	BA-SiO_2			−185.57			
	RHA-SiO_2			−164.20			
	Pure-SiO_2			−187.07			
ΔG° ($kJ{\cdot}mol^{-1}$)	BA-SiO_2	−5.60	−5.01	−3.93	−0.93	0.75	3.57
	RHA-SiO_2	−4.71	−4.19	−3.52	−0.33	1.75	2.72
	Pure-SiO_2	−6.94	−6.01	−5.07	−1.31	−0.008	1.64

third one (after 75 minutes) of adsorption equilibrium due to the much thicker solution layer on the surface of the adsorbent, which is expressed by a much higher C value. Furthermore, Table 5 indicates the decrease of k_{dif} values from k_{dif1} to k_{dif2} and k_{dif3}. Among them, a high k_{dif1} value refers to the external mass transfer to form a boundary layer on the surface of the material. The lower k_{dif2} value corresponds to the MB diffusion to the most internal adsorption sites of the adsorbent. Finally, k_{dif3} value might be close to zero because of the saturated adsorption sites [62].

3.5.5. Thermodynamic Study. The effect of temperature on the MB adsorption process onto synthesized nanosilica materials was studied with the aim of determining thermodynamic parameters describing the process with the investigated temperature range from 283 to 333 K. The exothermic or endothermic nature of adsorption is examined based on Van't Hoff equation as shown in equation (8), while equation (7) is the way to calculate the Gibbs free energy (ΔG°) of adsorption, in which the equilibrium constant of the process is inferred from equation (6) [50].

$$K_C = \frac{C_{ae}}{C_e} = \frac{C_o - C_e}{C_e}, \tag{6}$$

$$\Delta G^o = -\mathrm{RTK}_C, \tag{7}$$

$$\ln K_C = \frac{-\Delta G^o}{\mathrm{RT}} = \frac{\Delta S^o}{R} - \frac{\Delta H^o}{\mathrm{RT}}. \tag{8}$$

As shown in Table 6, the exothermic nature of MB adsorption onto three materials is inferred from all the negative values of standard enthalpy change. All the negative values of standard entropy change demonstrate that the reaction reduces the randomness of the system after the adsorption. Therefore, the mechanism of the process is predicted to be electrostatic bonding between MB^+ cations and the negatively charged surface of nanosilica as shown in Figure 15. This adsorption is spontaneous and favorable at temperatures lower than 323 K due to the negative value of the Gibbs free energy variations (ΔG°). From 323 K and up, the desorption rate is much higher than the adsorption one. As a result, ΔG° value exhibits positive values.

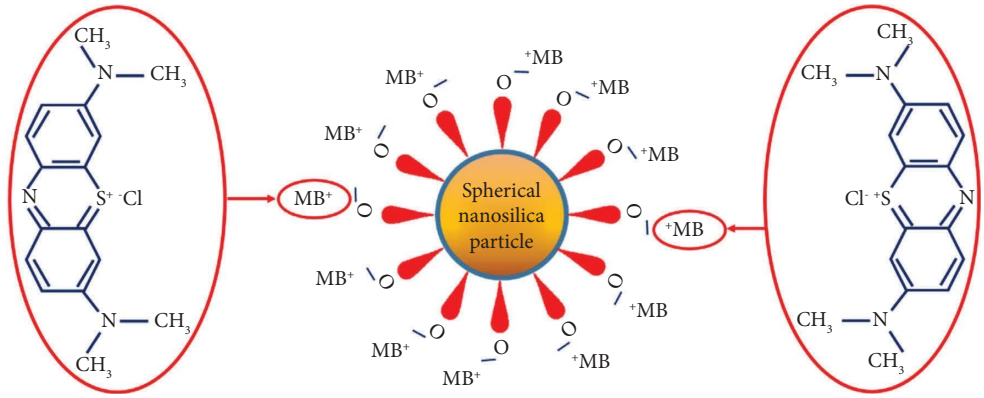

Figure 15: The proposed mechanism of MB adsorption onto nanosilica.

4. Conclusions

Nanosilica synthesized from rice husk and bagasse ashes was realized to be equivalent effective adsorbents for the removal of methylene blue from aqueous solution in comparison with nanosilica prepared from pure chemical. The three materials are favorably formed at a volume ratio of NH_4OH : ethanol of 12 : 3 and for 60 minutes of ultrasonic treatment. Most of MB was removed at ambient temperature with the three materials at a pH of 8 and adsorbent dosage of 0.375 g·L^{-1}. The isotherm data fitted well with the Freundlich model. The pseudo-second-order kinetic model well described the kinetic data, and the Weber model confirmed that the step-determining reaction rate is intraparticle diffusion. The increase of initial MB concentration results in the rising of adsorption equilibrium time. The adsorption mechanism of MB on the three nanosilica is the electrostatic bonding between MB^+ cations and the negatively charged surface of the nanosilica. The negative enthalpy (ΔH°) value demonstrates that the adsorption is an endothermic process. The adsorption is spontaneous in the range of temperature 283–313 K but unfavorable from 323 K.

Data Availability

The datasets generated during and/or analyzed during the current study are available from the corresponding author upon reasonable request.

Conflicts of Interest

The authors declare that they have no conflicts of interest.

Acknowledgments

This study was self-funded by the authors.

References

[1] R. Anliker and E. A. Clarke, "The ecology and toxicology of synthetic organic pigments," *Chemosphere*, vol. 9, no. 10, pp. 595–609, 1980.

[2] K. A. Moorthy, R. B. Govindarajan, S. P. Shukla, K. Kumar, and V. S. Bharti, "Acute toxicity of textile dye Methylene blue on growth and metabolism of selected freshwater microalgae," *Environmental Toxicology and Pharmacology*, vol. 82, Article ID 103552, 2020.

[3] M. N. Rashed, "Organic pollutants- monitoring, risk and treatment," *Adsorption Technique for the Removal of Organic Pollutants from Water and Wastewater*, BOD– Books On Demand, Norderstedt, Germany, 2013.

[4] D. Lan, H. Zhu, J. Zhang et al., "Adsorptive removal of organic dyes via porous materials for wastewater treatment in recent decades: a review on species, mechanisms and perspectives," *Chemosphere*, vol. 293, Article ID 133464, 2022.

[5] J. Liu, Z. Yu, Q. Li et al., "Adsorption behavior of gardenia yellow pigment on embedded spherical cellulose adsorbent," *RSC Advances*, vol. 11, no. 8, pp. 4407–4416, 2021.

[6] M. Meena, P. Sonigra, and G. Yadav, "Biological-based methods for the removal of volatile organic compounds (VOCs) and heavy metals," *Environmental Science and Pollution Research*, vol. 28, no. 3, pp. 2485–2508, 2020.

[7] D. Kanaujiya, T. Paul, A. Sinharoy, and K. Pakshirajan, "Biological treatment processes for the removal of organic micropollutants from wastewater: a review," *Current Pollution Reports*, vol. 5, no. 3, pp. 112–128, 2019.

[8] G. Zhu, Z. Yang, and X. Lu, "Removal characteristics of organic pollutants from eutrophic raw water by biological pretreatment reactors," *Journal of Chemistry*, vol. 2016, Article ID 3151482, 7 pages, 2016.

[9] S. Ledakowicz and K. Paździor, "Recent achievements in dyes removal focused on advanced oxidation processes integrated with biological methods," *Molecules*, vol. 26, no. 4, p. 870, 2021.

[10] A. Mojiri, A. Ohashi, N. Ozaki, A. Shoiful, and T. Kindaichi, "Pollutant removal from synthetic aqueous solutions with a combined electrochemical oxidation and adsorption method," *International Journal of Environmental Research and Public Health*, vol. 15, no. 7, p. 1443, 2018.

[11] F. E. Titchou, H. Zazou, H. Afanga et al., "Removal of organic pollutants from wastewater by advanced oxidation processes and its combination with membrane processes," *Chemical Engineering and Processing- Process Intensification*, vol. 169, Article ID 108631, 2021.

[12] M. de la Luz-Asunción, V. Sánchez-Mendieta, A. L. Martínez-Hernández, V. M. Castaño, and C. Velasco-Santos, "Adsorption of phenol from aqueous solutions by carbon nanomaterials of one and two dimensions: kinetic and equilibrium studies," *Journal of Nanomaterials*, vol. 2015, Article ID 405036, 14 pages, 2015.

[13] J. Zhou, Q. F. Lü, and J.-J. Luo, "Efficient removal of organic dyes from aqueous solution by rapid adsorption onto

polypyrrole–based composites," *Journal of Cleaner Production*, vol. 167, pp. 739–748, 2017.

[14] R. V. Kandisa, N. Saibaba Kv, K. B. Shaik, and R. Gopinath, "Dye removal by adsorption: a review," *Journal of Bioremediation and Biodegradation*, vol. 7, no. 6, 2016.

[15] A. A. Alshatwi, J. Athinarayanan, and V. S. Periasamy, "Biocompatibility assessment of rice husk-derived biogenic silica nanoparticles for biomedical applications," *Materials Science and Engineering: C*, vol. 47, pp. 8–16, 2015.

[16] J. Athinarayanan, V. S. Periasamy, M. Alhazmi, and A. A. Alshatwi, "Synthesis and biocompatibility assessment of sugarcane bagasse-derived biogenic silica nanoparticles for biomedical applications," *Journal of Biomedical Materials Research Part B: Applied Biomaterials*, vol. 105, no. 2, pp. 340–349, 2015.

[17] Y. Wang, Q. Zhao, N. Han et al., "Mesoporous silica nanoparticles in drug delivery and biomedical applications," *Nanomedicine: Nanotechnology, Biology and Medicine*, vol. 11, no. 2, pp. 313–327, 2015.

[18] M. Karnib, A. Kabbani, H. Holail, and Z. Olama, "Heavy metals removal using activated carbon, silica and silica activated carbon composite," *Energy Procedia*, vol. 50, pp. 113–120, 2014.

[19] A. B. Zeidman, O. M. Rodriguez-Narvaez, J. Moon, and E. R. Bandala, "Removal of antibiotics in aqueous phase using silica-based immobilized nanomaterials: a review," *Environmental Technology and Innovation*, vol. 20, Article ID 101030, 2020.

[20] M. Pishnamazi, A. Khan, T. A. Kurniawan, H. Sanaeepur, A. B. Albadarin, and R. Soltani, "Adsorption of dyes on multifunctionalized nano-silica KCC-1," *Journal of Molecular Liquids*, vol. 338, Article ID 116573, 2021.

[21] E. Da'na, "Nano-silica modified with diamine for capturing azo dye from aqueous solutions," *Molecules*, vol. 27, no. 11, p. 3366, 2022.

[22] G. Fan, M. Li, X. Chen, A. Palyanitsina, and A. Timoshin, "Polymer-Nanosilica-assisted to evaluate oil recovery performances in sandstone reservoirs," *Energy Reports*, vol. 7, pp. 2588–2593, 2021.

[23] E. Akhayere, A. Vaseashta, and D. Kavaz, "Novel magnetic nano silica synthesis using barley husk waste for removing petroleum from polluted water for environmental sustainability," *Sustainability*, vol. 12, no. 24, Article ID 10646, 2020.

[24] C. A. Franco, M. Martínez, P. Benjumea, E. Patiño, and F. B. Cortés, "Water remediation based on oil adsorption using nanosilicates functionalized with a petroleum vacuum residue," *Adsorption Science and Technology*, vol. 32, no. 2-3, pp. 197–207, 2014.

[25] G. Qu, J. Su, T. Shi, R. Guo, and J. Peng, "Effect evaluation of nanosilica particles on O/W emulsion properties," *Geofluids*, vol. 2022, Article ID 2339395, 10 pages, 2022.

[26] E. Akhayere and D. Kavaz, "Nano-silica and nano-zeolite synthesized from barley grass straw for effective removal of gasoline from aqueous solution: a comparative study," *Chemical Engineering Communications*, vol. 208, no. 10, pp. 1419–1435, 2021.

[27] S. Sabir, "Removal of motor oil using hydrophobic nanosilica," *Environmental Pollution and Protection*, vol. 2, no. 4, 2017.

[28] P. Zhang, N. Xie, X. Cheng, L. Feng, P. Hou, and Y. Wu, "Low dosage nano-silica modification on lightweight aggregate concrete," *Nanomaterials and Nanotechnology*, vol. 8, Article ID 184798041876128, 2018.

[29] H. Du, S. Du, and X. Liu, "Effect of nano-silica on the mechanical and transport properties of lightweight concrete," *Construction and Building Materials*, vol. 82, pp. 114–122, 2015.

[30] P. Sikora, T. Rucinska, D. Stephan, S.-Y. Chung, and M. Abd Elrahman, "Evaluating the effects of nanosilica on the material properties of lightweight and ultra-lightweight concrete using image-based approaches," *Construction and Building Materials*, vol. 264, Article ID 120241, 2020.

[31] L. Wang, C. Ning, T. Pan, and K. Cai, "Role of silica nanoparticles in abiotic and biotic stress tolerance in plants: a review," *International Journal of Molecular Sciences*, vol. 23, no. 4, p. 1947, 2022.

[32] M. El-Naggar, N. R. Abdelsalam, M. M. G. Fouda et al., "Soil application of nano silica on maize yield and its insecticidal activity against some stored insects after the post-harvest," *Nanomaterials*, vol. 10, no. 4, p. 739, 2020.

[33] V. H. Le, C. N. H. Thuc, and H. H. Thuc, "Synthesis of silica nanoparticles from Vietnamese rice husk by sol–gel method," *Nanoscale Research Letters*, vol. 8, no. 1, p. 58, 2013.

[34] X.-D. Wang, Z.-X. Shen, T. Sang et al., "Preparation of spherical silica particles by Stöber process with high concentration of tetra-ethyl-orthosilicate," *Journal of Colloid and Interface Science*, vol. 341, no. 1, pp. 23–29, 2010.

[35] A. N. Azzahra, E. S. Yusefin, G. Salima, M. M. W. M. Mudita, N. A. Febriani, and A. B. D. Nandiyanto, "Review: synthesis of nanosilica materials from various sources using various methods," *Journal of Applied Sciences in Environmental Sanitation*, vol. 3, no. 4, pp. 254–278, 2020.

[36] C. Real, D. Alcala, J. M. Criado, and M. Jose, "Preparation of silica from rice husks," *Journal of the American Ceramic Society*, vol. 79, no. 8, pp. 2012–2016, 1996.

[37] Y. M. Z. Ahmed, E. Ewais, and Z. I. ZaKi, "Production of porous silica by the combustion of rice husk ash for tundish lining," *Journal of University of Science and Technology Beijing, Mineral, Metallurgy, Material*, vol. 15, no. 3, pp. 307–313, 2008.

[38] R. Khan, A. Jabbar, I. Ahmad, W. Khan, A. N. Khan, and J. Mirza, "Reduction in environmental problems using rice-husk ash in concrete," *Construction and Building Materials*, vol. 30, pp. 360–365, 2012.

[39] M. Noushad, I. A. Rahman, A. Husein, D. Mohamad, and A. R. Ismail, "A simple method of obtaining spherical nanosilica from rice husk," *International Journal of Advanced Science, Engineering and Information Technology*, vol. 2, no. 2, pp. 141–230, 2012.

[40] I. M. Joni, Rukiah, and C. Panatarani, "Synthesis of silica particles by precipitation method of sodium silicate: effect of temperature, pH and mixing technique," *AIP Conference Proceedings*, vol. 2219, Article ID 80018, 2020.

[41] N. Setyawan, Hoerudin, and S. Yuliani, "Synthesis of silica from rice husk by sol-gel method," *IOP Conference Series: Earth and Environmental Science*, vol. 733, no. 1, Article ID 12149, 2021.

[42] M. Nasiruddin Khan and A. Sarwar, "Determination of points of zero charge of natural and treated adsorpbents," *Surface Review and Letters*, vol. 14, no. 3, pp. 461–469, 2007.

[43] S. Sompech, T. Dasri, and S. Thaomola, "Preparation and characterization of amorphous silica and calcium oxide from agricultural wastes," *Oriental Journal of Chemistry*, vol. 32, no. 4, pp. 1923–1928, 2016.

[44] G. Yang, W. Lin, H. Lai et al., "Understanding the relationship between particle size and ultrasonic treatment during the synthesis of metal nanoparticles," *Ultrasonics Sonochemistry*, vol. 73, Article ID 105497, 2021.

[45] S. K. Bhangu, A. Baral, H. Zhu, M. Ashokkumar, and F. Cavalieri, "Sound methods for the synthesis of nanoparticles from biological molecules," *Nanoscale Advances*, vol. 3, no. 17, pp. 4907–4917, 2021.

[46] S. Khurana, S. Negi, and A. Chandra, "Effect of surface modification of dispersoid on hybrid polymer electrolyte," *Polymer Testing*, vol. 96, Article ID 107118, 2021.

[47] K. A. Cychosz and M. Thommes, "Progress in the physisorption characterization of nanoporous gas storage materials," *Engineering*, vol. 4, no. 4, pp. 559–566, 2018.

[48] R. Dong, L. Wang, J. Zhu, L. Liu, and Y. Qian, "A novel SiO2-GO/acrylic resin nanocomposite: fabrication, characterization and properties," *Applied Physics A*, vol. 125, no. 8, p. 551, 2019.

[49] S. Saravanan and R. S. Dubey, "Synthesis of SiO2 nanoparticles by sol-gel method and their optical and structural properties," *Romanian Journal of Information Science and Technology*, vol. 23, no. 1, pp. 105–112, 2020.

[50] D. V. Q. Nguyen, Q. K. Dinh, N. T. Tran, X. T. Dang, and T. H. D. Bui, "Carbon nanotubes: synthesis via chemical vapour deposition without hydrogen, surface modification, and application," *Journal of Chemistry*, vol. 2019, Article ID 4260153, 14 pages, 2019.

[51] R.-L. Tseng and F.-C. Wu, "Inferring the favorable adsorption level and the concurrent multi-stage process with the Freundlich constant," *Journal of Hazardous Materials*, vol. 155, no. 1-2, pp. 277–287, 2008.

[52] K. Moeinian and S. M. Mehdinia, "Removing methylene blue from aqueous solutions using rice husk silica adsorbent," *Polish Journal of Environmental Studies*, vol. 28, no. 4, pp. 2281–2287, 2019.

[53] F. Salimi, K. Tahmasobi, C. Karami, and A. Jahangiri, "Preparation of modified nano-SiO2 by bismuth and iron as a novel remover of methylene blue from water solution," *Journal of the Mexican Chemical Society*, vol. 61, no. 3, pp. 250–259, 2017.

[54] D. Ingrachen-Brahmi, H. Belkacemi, and L. Ait Brahem-Mahtout, "Adsorption of Methylene Blue on silica gel derived from Algerian siliceous by- product of kaolin," *Journal of Materials and Environmental Science*, vol. 11, no. 7, pp. 1044–1057, 2020.

[55] R. Chueachot, S. Wongkhueng, K. Khankam et al., "Adsorption efficiency of methylene blue from aqueous solution with amine-functionalized mesoporous silica nanospheres by co-condensation biphasic synthesis: adsorption condition and equilibrium studies," *Materials Today: Proceedings*, vol. 5, no. 6, pp. 14079–14085, 2018.

[56] A. A. Almethen, K. M. Alotaibi, H. S. Alhumud, and A. M. Alswieleh, "Highly efficient and rapid removal of methylene blue from aqueous solution using folic acid-conjugated dendritic mesoporous silica nanoparticles," *Processes*, vol. 10, no. 4, p. 705, 2022.

[57] Z.-H. Yu, S.-R. Zhai, H. Guo et al., "Removal of methylene blue over low-cost mesoporous silica nanoparticles prepared with naturally occurring diatomite," *Journal of Sol-Gel Science and Technology*, vol. 88, no. 3, pp. 541–550, 2018.

[58] V. Krstić, "Role of zeolite adsorbent in water treatment," *Handbook of Nanomaterials for Wastewater Treatment, Fundamentals and Scale Up Issues Micro and Nano Technologies*, pp. 417–481, 2021.

[59] D. V. Q. Nguyen, N. T. Tran, Q. K. Dinh et al., "Lead ions removal from aqueous solution using modified carbon nanotubes," *Bulletin of Materials Science*, vol. 41, no. 1, pp. 1–11, 2018.

[60] W. J. Weber and J. C. Morris, "Kinetics of adsorption on carbon from solution," *Journal of the Sanitary Engineering Division*, vol. 89, no. 2, pp. 31–59, 1963.

[61] H. K. Agbovi and L. D. Wilson, "Adsorption processes in biopolymer systems: fundamentals to practical applications," *Natural Polymers-Based Green Adsorbents for Water Treatment*, pp. 1–51, 2021.

[62] N. F. Compos, C. Mbm Barbosa, J. M. Rodríguez-Díaz, and M. Mmb Duarte, "Removal of naphthenic acids using activated charcoal: kinetic and equilibrium studies," *Adsorption Sicence and Technology*, vol. 36, no. 7-8, pp. 1–17, 2018.